NASA TM- 85943

NASA Technical Memorandum 85943

USAAVSCOM Technical Report 84-A-1

FOR REFERENCE

NOT TO BE TAKEN FROM THIS ROOM

NASA-TM-85943

19840023484

Calculation of Boundary Layers of Oscillating Airfoils

Tuncer Cebeci and Lawrence W. Carr

May 1984

LIBRARY COPY

AUG 2 1984

LANGLEY RESEARCH CENTER
LIBRARY, NASA
HAMPTON, VIRGINIA

National Aeronautics and
Space Administration

United States Army
Aviation Systems
Command

NF00804

NASA Technical Memorandum 85943

USAAVSCOM Technical Report 84-A-1

Calculation of Boundary Layers of Oscillating Airfoils

Tuncer Cebeci, Mechanical Engineering Department, California State University
Long Beach, California

Lawrence W Carr, Ames Research Center and Aeromechanics Laboratory, U S Army
Research and Technology Laboratories - AVSCOM, Ames Research
Center, Moffett Field, California

NASA

National Aeronautics and
Space Administration

Ames Research Center
Moffett Field, California 94035

United States Army
Aviation Systems
Command
St Louis, Missouri 63120

N84-31554#

CALCULATION OF BOUNDARY LAYERS OF OSCILLATING AIRFOILS

Tuncer Cebeci* and Lawrence W. Carr**

ABSTRACT

A two-point finite difference unsteady laminar and turbulent boundary layer computational method has been used to investigate the properties of the flow around an airfoil (NACA 0012) oscillating through angles of attack up to 18 degrees, for reduced frequencies of 0.01 and 0.20. The unsteady potential flow was determined using the unsteady potential flow method of Geissler. The influence of transition location on stall behavior was investigated, using both experimentally determined transition information, and transition located at the pressure peak; the results show the need for viscous-inviscid interaction in future computation of such flows.

---

*Mechanical Engineering Dept., California State University, Long Beach, CA 90840.

**Ames Research Center and Aeromechanics Laboratory, AVRADCOM Research and Technology Laboratories, Moffett Field, California.

INTRODUCTION

Present knowledge of steady boundary-layer flows is considerable and stems from exhaustive investigation over almost eighty years. In contrast, unsteady boundary-layer flows have received slight attention and only in the recent past. The requirements imposed by the need to improve the performance of helicopter rotors, wind-energy devices and hydrofoil characteristics imply the need for further research. This is particularly so since many of the unsteady flow investigations have been concerned with detail such as the existence or the nonexistence of singularity and its structure, see for example the papers contained in ref. 1. Here we are concerned with aspects of our ability to calculate the flow properties around oscillating airfoils in a range of parameters of direct relevance to engineering practice.

The need for further development of boundary-layer procedures to represent unsteady flows is clear from the recent experiments of McCroskey et al.[2], Tijdeman[3], Davis and Malcolm[4], Cousteix et al.[5], Carr et al.[6], Young [7], Carr and McAlister[8] and Geissler[9]. The range of measurements is reasonably extensive and includes subsonic and transonic flow, a range of airfoil sections and

parameters of unsteady motion. Four flow regimes have been identified[10] and correspond to no stall, stall onset, light stall and deep stall. None of these regimes nor the apparent breakdown of the unsteady boundary layer to form a large vortex near the surface at large angle of attack have been represented satisfactorily by calculation methods.

Previous attempts to calculate oscillating airfoil flows have involved either the solution of Navier-Stokes equations, Mehta [11] and Shamroth[12] or the solution of the boundary-layer equations, Cebeci and Carr[13,14] and Geissler[15]. While both approaches have merits, it is clear that the latter procedure, with further development, is likely to allow more precise solution of the equations and economy of computer resources.

The calculation of boundary-layers on an oscillating airfoil differs from the usual nonoscillating airfoil-flow calculations in that difficulties are caused by the translation of the stagnation point in space and time. In particular, it is necessary to develop a procedure to generate initial conditions in the immediate vicinity of the moving stagnation point and to account for the flow reversal that occurs in this region. In reference 14, the present authors described two procedures for generating initial conditions near the stagnation point of an oscillating airfoil. The first procedure used the characteristic box scheme and was shown to be accurate and free from the limitations which may be imposed by the flow reversal. The second procedure used a quasi-steady approach and was also shown to be appropriate provided that the region where it was used was far from any flow reversal.

The work described here is the continuation of that of reference 14, and explores the calculation of laminar and turbulent boundary layers on the whole oscillating airfoil. It has three separate but related phases. First, it is necessary to conduct numerical tests of the procedures of ref. 14 and of the

boundary conditions generated by the potential flow code of ref. 16. Secondly, oscillating airfoils involve transition from laminar to turbulent flow and the data provided by Carr and his coworkers allow the direct evaluation of transition assumptions which must be made in the boundary-layer calculations. In particular, a simple assumption is to involve transition at the location corresponding to the peak pressure calculated by the inviscid flow method. The available experimental data permit the implications of this assumption to be evaluated and compared with those empirical transition methods used for steady flows and described in ref. 17. Thirdly, leading edge separation bubbles and trailing edge separation can also occur at higher angles of attack as demonstrated by Carr et al.[6] The ability of a calculation method to represent these regions of separation and the expressions used to model turbulent flows at low Reynolds numbers with separation as well as transitional flows need to be investigated.

The study reported here is continuing and this contribution may be regarded as a report of progress since that of ref 14.

BASIC EQUATIONS

Boundary-Layer Equations

The boundary-layer equations for an incompressible laminar or turbulent flow on an oscillating airfoil are well known and, with the eddy viscosity concept, can be written as

$$\frac{\partial u}{\partial x} + \frac{\partial v}{\partial y} = 0 \tag{1}$$

$$\frac{\partial u}{\partial t} + u\frac{\partial u}{\partial x} + v\frac{\partial u}{\partial y} = \frac{\partial u_e}{\partial t} + u_e\frac{\partial u_e}{\partial x} + \frac{\partial}{\partial y}\left(b\frac{\partial u}{\partial y}\right) \tag{2}$$

Here x denotes distance along the surface of the airfoil, y along the normal and $b = \nu + \varepsilon_m$. In the absence of mass transfer, Eqs. (1) and (2) are subject to boundary conditions given by

$$y = 0; \qquad u = v = 0: \qquad y = \delta, \qquad u = u_e(x,t) \tag{3}$$

The presence of the eddy viscosity ε_m requires a turbulence model and we use the algebraic eddy-viscosity formulation developed by Cebeci and Smith (ref. 18). According to this formulation ε_m is defined by two separate formulas. In the inner region of the boundary layer $(\varepsilon_m)_i$ is defined as:

$$(\varepsilon_m)_i = \{0.4y[1 - \exp(-y/A)]\}^2 \left|\frac{\partial u}{\partial y}\right| \gamma_{tr} \qquad 0 \leq y \leq y_c \tag{4}$$

where

$$A = 26\nu u_\tau^{-1} [1 - 11.8\ p^+]^{-1/2}, \qquad u_\tau = \left(\frac{\tau}{\rho}\right)_{max}^{1/2}, \qquad p^+ = \frac{\nu u_e}{u_\tau^3} \frac{\partial u_e}{\partial x} \tag{5}$$

In Eq. (4), γ_{tr} is an intermittency factor that accounts for the transitional region that exists between a laminar and turbulent flow. It is defined by

$$\gamma_{tr} = 1 - \exp\left[-G\ (x - x_{tr}) \int_{x_{tr}}^{x} \frac{d\xi}{u_e}\right] \tag{6}$$

Here x_{tr} is the location of the start of transition and the empirical factor G which has the dimensions of velocity/(length)^2, is given by (ref. 18)

$$G = \frac{1}{1200} \frac{u_e^3}{\nu^2} R_{x_{tr}}^{-1.34} \tag{7}$$

The transition Reynolds number is defined as $R_{x_{tr}} = (u_e x/\nu)_{tr}$.

In the outer region $(\varepsilon_m)_o$ is defined by:

$$(\varepsilon_m)_o = 0.0168 \left| \int_0^\infty (u_e - u)dy \right| \gamma_{tr} \qquad y_c \leq y \leq \infty \tag{8}$$

The boundary between the inner and outer regions, y_c, is established by the continuity of the eddy-viscosity formulas.

Initial Conditions

If initial conditions in the (t,y) plane are given at a station x_0 on the upper surface of the airfoil and satisfy the condition $u > 0$ and, in addition, initial conditions are given in the (x,y) plane at $t = 0$, then the solution of Eqs. (1), (2) and (3) may be obtained for $x > x_0$ and $t > 0$ until they breakdown (flow separation). A similar remark applies to the lower surface except that $u < 0$. The initial conditions at $t = 0$ can be generated for both surfaces if steady conditions are assumed to prevail at that time. It is only necessary to solve the appropriate equations which, in this case, are given by Eq. (1) and by

$$u \frac{\partial u}{\partial x} + v \frac{\partial u}{\partial y} = u_e \frac{du_e}{dx} + \frac{\partial}{\partial y} \left(b \frac{\partial u}{\partial y}\right) \tag{9}$$

There is no problem with the initial conditions for Eqs. (1) and (9) since the calculations start at the stagnation point $x = x_s$, where u_e and u are zero for all y.

Unlike steady flows, where u_e and u are zero for all y at the stagnation point, the stagnation point is not fixed in an unsteady flow; although u_e is zero, we cannot assume a priori that u is also zero. We may avoid these difficulties by using an implicit method, but now we are faced with the problem of generating a starting profile on the new time line. A convenient and accurate procedure to calculate the first velocity profile at the new time-line has been developed by the present authors as described in ref. 14; it involves the use of the Characteristic Box scheme developed by Cebeci and Stewartson (ref. 19). Another procedure is to use a quasi-steady

approach in the immediate vicinity of the stagnation point. As long as the region where this approach is used does not contain flow separation, it is simpler to use than the first approach which employs the characteristic-box scheme. As a result, it is used here.

Transformed Equations

As in previous studies (see, for example, ref. 17), we use similarity variables to transform the governing equations before we seek their solution. For a steady flow, we use the Falkner-Skan transformation defined by

$$\eta = \sqrt{\frac{u_e}{\nu x}}\, y, \qquad \psi = \sqrt{u_e \nu x}\, f(x,\eta) \tag{10}$$

where ψ is the usual definition of stream function that satisfies the continuity equation, Eq. (1), that is

$$u = \frac{\partial \psi}{\partial y}, \qquad v = -\frac{\partial \psi}{\partial x} \tag{11}$$

With this transformation, Eq. (9) and its boundary conditions, Eq. (3), can be written as

$$(bf'')' + \frac{m+1}{2} ff'' + m[1 - (f')^2] = x\left(f' \frac{\partial f'}{\partial x} - f'' \frac{\partial f}{\partial x}\right) \tag{12}$$

$$\eta = 0; \qquad f = f' = 0: \qquad \eta = \eta_e; \qquad f' = 1 \tag{13}$$

where primes denote differentiation with respect to η, m denotes a dimensionless pressure-gradient parameter defined by

$$m = \frac{x}{u_e} \frac{du_e}{dx} \tag{14a}$$

and b is defined by

$$b = 1 + \varepsilon_m^+, \qquad \varepsilon_m^+ = \varepsilon_m/\nu \tag{14b}$$

For unsteady flows, we use a transformation similar to that defined by Eq. (10) except that u_e is now a function of both x and t and the dimensionless stream function F is a function of x, t and ζ; we let

$$\zeta = \sqrt{\frac{u_e(x,t)}{\nu x}}\, y, \qquad \psi = \sqrt{u_e(x,t)\nu x}\; F(x,t,\zeta) \tag{15}$$

With this transformation it can be shown that the continuity and momentum equations and their boundary conditions for unsteady incompressible flows can be written as

$$(bF'')' + \frac{n+1}{2} FF'' + m[1 - (F')^2] + m_3(1 - F') - \frac{\zeta}{2} m_3 F'' =$$

$$x\left[\frac{1}{u_e}\frac{\partial F'}{\partial t} + F'\frac{\partial F'}{\partial x} - F''\frac{\partial F}{\partial x}\right] \tag{16}$$

$$\zeta = 0; \qquad F = F' = 0: \qquad \zeta = \zeta_e; \qquad F' = 1 \tag{17}$$

Here primes now denote differentiation with respect to ζ and

$$m = \frac{x}{u_e}\frac{\partial u_e}{\partial x}, \qquad m_e = \frac{x}{u_e^2}\frac{\partial u_e}{\partial t} \tag{18}$$

Solution Procedure

We use Keller's Box method to solve the governing equations of the previous section. This is a two-point finite-difference method which has been used to solve a wide range of parabolic partial-differential equations as discussed in ref. 19. The solution procedure for Eqs. (12) and (13) is identical to that described in ref. 17. The solution procedure used to generate the initial conditions in the (x,y) and (t,y) planes is described in reference 13. For unsteady flows, where we now solve Eqs. (16) and (17), we use the solution procedure described in ref. 20. In regions where there are no flow reversals across the layer, we use the Standard Box scheme and in regions where there is flow reversal, we use the Zig-Zag scheme.

RESULTS AND DISCUSSION

To accomplish the objectives stated in the Introduction with the boundary-layer method discussed in the previous section, we have considered the NACA 0012 airfoil and calculated its pressure distribution with Geissler's inviscid code[16] for two reduced frequencies, k = 0.01 and k = 0.20 and for two angles of attack

$$\alpha = \begin{cases} 5^\circ + 5^\circ \sin\omega t & \text{(19a)} \\ 8^\circ + 10^\circ \sin\omega t & \text{(19b)} \end{cases}$$

The experimental data taken for these two angles of attack and two frequencies show that the one with the smaller variation in angle of attack, Eq. (19a), has no trailing-edge separation on the whole airfoil for either frequency. Its maximum angle of attack range falls in what McCroskey and Pucci call the "no stall region" ($\alpha_{max} < 13^\circ$). The only flow separation occurs in the form of a bubble near the upper surface leading edge. For $\alpha \geq 5^\circ$, flow separates and reattaches as the flow goes from laminar to turbulent.

The flow corresponding to the larger variation in angle of attack, Eq. (19b), on the other hand, has a leading edge separation bubble as well as an open trailing edge separation. Its maximum angle of attack range falls in between light stall ($\alpha_{max} < 15^\circ$) and deep stall ($\alpha_{max} < 20^\circ$) with the magnitude of reduced frequency playing an important role in the performance of airfoil characteristics. As discussed by McCroskey and Pucci[10], the qualitative behavior of light stall in this case is sensitive to reduced frequency and maximum incidence for a specified airfoil at zero Mach number. The qualitative behavior is closely related to the boundary-layer separation characteristics (leading-edge vs trailing-edge separation) and to the changes in this separation behavior α_{max} and k. An important point that they note

is the amount of trailing-edge separation suppressed by increasing the frequency. As a result of this unsteady effect, an airfoil that falls in the light stall region can pass from light-stall with $k \leq 0.10$ to stall onset ($\alpha_{max} = 14$) for $k \geq 0.15$.

The boundary-layer method described in the previous section is able to calculate both laminar and turbulent flows. The calculations start at the stagnation point for the given pressure distribution and for the specified freestream. The initial conditions at $t = 0$ are obtained by solving the steady flow form of the equations and those in the (t,y) plane with the quasi-steady approach described earlier and applied only in the immediate neighborhood of the stagnation region. Transition is achieved by specifying its location as part of the input to the computer program. In contrast to steady flows where empirical correlations for transition have been developed and compared satisfactorily with experimental data, little is known of the same phenomena in unsteady flows. Here we have taken two approaches. In the first, if available, transition location has been specified directly from experiment and in the second it has been specified at the location of maximum pressure. The first assumption allows the evaluation of the numerical technique and the second is expected to be physically sound since the pressure distribution becomes increasingly peaky as the angle of attack is increased and the merits of this assumption can be tested. It can also be expected that the second assumption will become less appropriate as the peak in the pressure distribution diminishes with decreasing angle of attack.

Figures 1 and 2 show the variation of displacement thickness δ^*, and local skin-friction coefficient, c_f, distributions on the airfoil at different angles of attack for two reduced frequencies. Here δ^* and c_f are defined by

$$\delta^* = \int_0^\infty (1 - \frac{u}{u_e})dy, \qquad c_f = \frac{2\tau_w}{\rho u_e^2} \tag{20a}$$

and in terms of the transformation given by Eq. (15) can be expressed as

$$\delta^* = \frac{x}{\sqrt{R_x}} (\eta_e - F_e), \qquad c_f = \frac{2F''_w}{\sqrt{R_x}} \tag{20b}$$

Transition was assumed to correspond to maximum pressure and the chord Reynolds number, R_c, was taken as 3×10^6 and approximately 100 stations were taken in the x-direction with 41 stations in the time direction corresponding to $\Delta\omega t = 9°$. The steady-state conditions were obtained from the pressure distribution that corresponded to $\alpha = 0$ by taking $\omega t = 270°$ and the calculations for $t > 0$ were performed for increasing angle of attack. Since we are using an unsteady pressure distribution to calculate the initial conditions at $t = 0$ and $\partial u/\partial t$ is not zero at $t = 0$, slight oscillation occurs when unsteady-flow calculations are performed for the next time step. For this reason a smoothing procedure was applied to the calculated results at that time station and the next few stations.

As can be seen from the results, there is no flow separation on the airfoil except for a very small region at the trailing edge. This is without doubt due to the inaccuracy of the inviscid pressure distribution in that region where the effect of viscous forces on the inviscid flow is greatest. An inviscid-viscous interaction should eliminate the trailing-edge separation.

The calculations for case 2 are more difficult to perform than those for case 1 since the flow regime falls between light stall and deep stall, due to larger variations in angle of attack. Whereas there is almost no flow separation in case 1, there is both leading-edge and trailing-edge separation for case 2. Once the calculations have started for steady state for, say ωt corresponding to 270°, we expect that flow separation will take place as the

angle of attack increases. However, whether the first flow separation will manifest itself in the form of leading-edge separation or trailing-edge separation remains to be explored. In either case, if the flow separates at the leading-edge at higher angles of attack, then the use of the boundary-layer method will lead to breakdown of the solutions due to the singularity at separation, and, as a result, calculations cannot be performed for the downward stroke beyond the separation point. For the case when the separation takes place near the trailing edge, again the calculations cannot be extended beyond the separation point for the downward stroke.

The calculations for case 2 were again performed for the same chord Reynolds number and for the same number of x- and t-stations. The initial calculations were started by using the pressure distribution which corresponded to $\alpha = -2°$. Transition locations were specified by two different approaches for two reduced frequencies, $k = 0.01$ and $k = 0.20$.

Figure 3 shows the variation of transition as a function of angle of attack for case 2 at two frequencies. We see from these figures that the effect of reduced frequency on the location of transition is considerable. At the lower frequency, transition occurs almost at the same location on the upward and downward strokes whereas, with the higher frequency, the transition locations on both strokes differ noticeably. Compared with the lower frequency case, with increasing frequency, the transition location moves backward in the upward stroke and forward in the downward stroke. It is obvious that a correct prediction of airfoil characteristics in the same angle of attack range for different frequencies will depend on our ability to predict transition as a function of frequency among other things.

Figures 4 to 8 show the results for case 2. Those in Figures 4 and 5 correspond to a transition location at the maximum pressure peak. The first traces of flow reversal occur near the trailing edge at $\alpha \simeq 8°$ and are

limited to less than the chord length. As the angle of attack increases, the flow reversal region near the trailing edge slightly increases becoming approximately 5% at $\alpha = 18°$. There is no leading-edge separation for either frequency.

Figure 6 shows the results for case 2 in which transition locations were input from the experimental data, according to Fig. 3b. Again the calculations were started at the same angle of attack, $\alpha = -2$, and continued in the upward stroke mode. In this case, however, the solutions broke down at $\alpha = 11.09°$. There was essentially no flow reversal and no signs of numerical difficulties until $\alpha = 9.54$ when flow separation appeared around the trailing edge. At the next angle of attack, $\alpha = 11.09$, a laminar leading-edge separation bubble appeared at around 4% chord and the solutions broke down shortly thereafter. Figure 6 also shows that while the computed displacement thickness distributions are smooth, those corresponding to local skin friction are not. The wiggles in the latter case are a result of transition locations specified at different angles of attack. For example, we see from Figure 3b that for $-2 \leq \alpha \leq 0$, the transition location moves from $(x/c)_{tr} = 0.40$ to approximately $(x/c)_{tr} = 0.55$. This means that the laminar flow calculations for $\alpha = 0$ contain a combination of laminar and turbulent flow characteristics which originated at $\alpha = -2$ where the laminar flow calculations terminated at $(x/c)_{tr} = 0.40$.

Calculations were also performed with the transition criterion of Michel, which was devised for steady flows, and the results were found to be similar to those of Figure 6 except that the solutions broke down earlier at $\alpha = 8°$. Figure 7 allows comparison between the measured transition locations and those calculated from Michel's formula during the upward stroke together with those corresponding to maximum pressure peak. It is clear, therefore, that the use

of this correlation, although imperfect, is to be preferred to the specification of transition at the location of the pressure peak.

The intermittency expression used for the transitional region in the eddy-viscosity formula can play an important role in the calculation of leading-edge separation bubbles. It is likely that this formula, which has been used satisfactorily for attached flows undergoing transition from laminar to turbulent flows, may not be as accurate for flows undergoing transition due to separation. It is evident from Eqs. (6) and (7) that the coefficient of the parameter G controls the transition length. Thus a decrease in G by a factor of 10 will reduce the transition length which, in turn, will lessen the possibility of separation. Calculations shown in Figure 8 performed with a value of 1/120 for the coefficient of G revealed that the leading-edge separation had been suppressed allowing the calculations to proceed and to reveal trailing-edge separation. This procedure permitted the calculations to be performed in the upward stroke to an angle of 18° where the trailing-edge separation had moved forward to around 20% chord. This sensitivity of the calculated flow to the coefficient of G requires further confirmation which may be obtained, in part, by the use of interactive methods; in this way the breakdown caused by the singularity will no longer occur.

CONCLUDING REMARKS

The numerical method of ref. 13 has been used to investigate the properties of the flow around an airfoil (NACA 0012) oscillating with angles of attack up to 18° and for reduced frequencies of 0.01 and 0.20. This encompasses the regions of no-stall and deep stall identified by McCroskey and Pucci[10]. The inviscid pressure distribution was obtained from Geissler's method. The calculations were performed without numerical difficulties in

both flow regimes and the zig-zag numerical scheme was shown to work satisfactorily in regions of flow reversal.

The influence of transition location was investigated with the numerical method. The specification of transition at the location of pressure peak led to results which were in disagreement with experiment for the low frequency case; in particular, the calculated results did not reveal the deep stall observed in ref. 10. In contrast, the results for the high frequency case were in accord with experiment. Use of the experimentally determined transition location for the high frequency case, however, led to discrepancies which may well be attributed to the pressure distribution obtained from inviscid-flow theory which does not consider any separation on the airfoil. This suggests the need for interaction between the viscous and inviscid flow calculations.

Further investigations were conducted with the turbulence model of Cebeci and Smith which includes consideration of the transition region. It was found that the length of the transition region could be controlled by modifications to the model with consequent reduction of the transition region and of the separation bubble. Additional studies are required to quantify the effects, and, once again, should make use of interactive procedures.

5.0 REFERENCES

1. Cebeci, T. (Ed.): Numerical and Physical Aspects of Aerodynamic Flows, Part 3, Springer-Verlag, NY, 1982.
2. McCroskey, W.J., McAlister, K.W., Carr, L.W. and Pucci, S.L.: An Experimental Study of Dynamic Stall on Advanced Airfoil Sections 1, 2, 3. NASA TM-84245, 1982.
3. Tijdeman, H.: Investigations of the Transonic Flow Around Oscillating Airfoils. NLR TR 77090U, 1977.

4. Davis, S.S. and Malcolm, G.N.: Experiments in Transonic Flow. AIAA Paper 79-769, 1979.

5. Cousteix, J., Houdeville, R. and Janelle, J.: Response of a Turbulent Boundary Layer to a Pulsation of the External Flow With and Without Adverse Pressure Gradient. In Unsteady Turbulent Shear Flows (ed. R. Michel, J. Cousteix, R. Houdeville) Springer-Verlag, 120-144, 1981.

6. Carr, L.W., McAlister, K.W. and McCroskey, W.J.: Analysis of the Development of Dynamic Stall Based on Oscillating Airfoil Experiments. NASA TN D-8382, 1977.

7. Young, W.H., Jr.: Fluid-Mechanics Mechanisms in the Stall Process of Airfoils for Helicopters. In Numerical and Physical Aspects of Aerodynamic Flows (ed. T. Cebeci), 601-615, 1982.

8. Carr, L.W. and McAlister, K.W.: The Effect of a Leading-Edge Slat on the Dynamic Stall of an Oscillating Airfoil. AIAA Paper 83-2533, 1983.

9. Geissler, W.: Theoretical and Experimental Dynamic Stall, Investigations on a Rotor Tip Blade. Second Symposium on Numerical and Physical Aspects of Aerodynamic Flows, Long Beach, CA, 1983.

10. McCroskey, W.J. and Pucci, S.L.: Viscous-Inviscid Interaction on Oscillating Airfoils in Subsonic Flow. AIAA J., Vol. 20, 167-174, 1982.

11. Mehta, U.: Dynamic Stall of an Oscillating Airfoil. AGARD Conf. Proceedings No. 227, Paper No. 23, 1977.

12. Shamroth, S.J.: A Turbulent Flow Navier-Stokes Analysis for an Airfoil Oscillating in Pitch. In Unsteady Turbulent Shear Flows (ed. R. Michel, J. Cousteix, R. Houdeville), 185-196, 1981.

13. Cebeci, T. and Carr, L.W.: Prediction of Boundary-Layer Characteristics of an Oscillating Airfoil. In Unsteady Turbulent Shear Flows (ed. R. Michel, J. Cousteix, R. Houdeville), 145-158, 1981.

14. Cebeci, T. and Carr, L.W.: Calculation of Boundary Layers Near the Stagnation Point of an Oscillating Airfoil. NASA TM 84305, 1983.

15. Geissler, W.: Unsteady Laminar Boundary-Layer Calculations on Oscillating Configurations Including Backflow. Part II: Airfoil in High-Amplitude Pitching Motion - Dynamic Stall. NASA TM 84319, 1983.

16. Geissler, W.: Private communication, 1983.

17. Cebeci, T. and Bradshaw, P.: Momentum Transfer in Boundary Layers. McGraw-Hill/Hemisphere, Washington, DC, 1977.

18. Cebeci, T. and Smith, A.M.O.: Analysis of Turbulent Boundary Layers, Academic Press, NY, 1974.

19. Bradshaw, P., Cebeci, T. and Whitelaw, J.H.: Engineering Calculation Methods for Turbulent Flows. Academic Press, London, 1981.

20. Cebeci, T. and Carr, L.W.: Computation of Unsteady Turbulent Boundary Layers with Flow Reversal and Evaluation of Two Separate Turbulence Models. USAAVRADCOM TR 81-A-5.

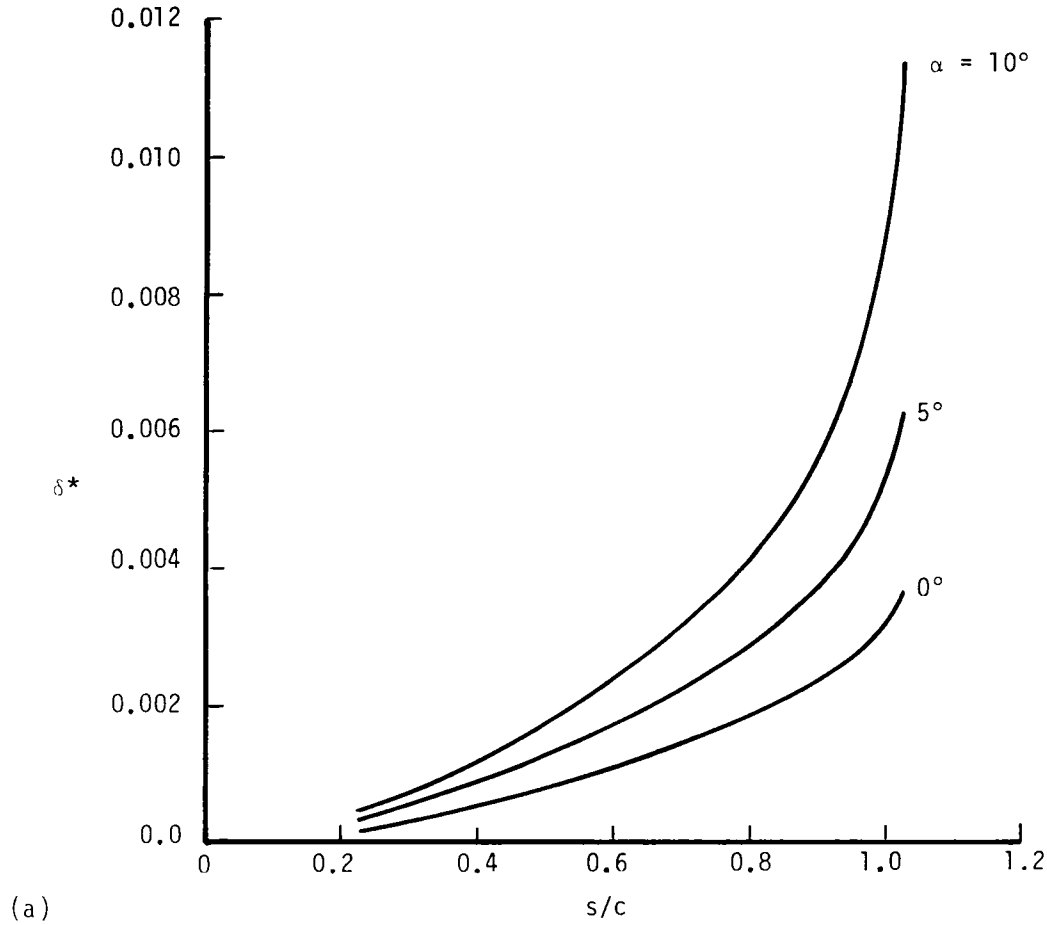

(a)

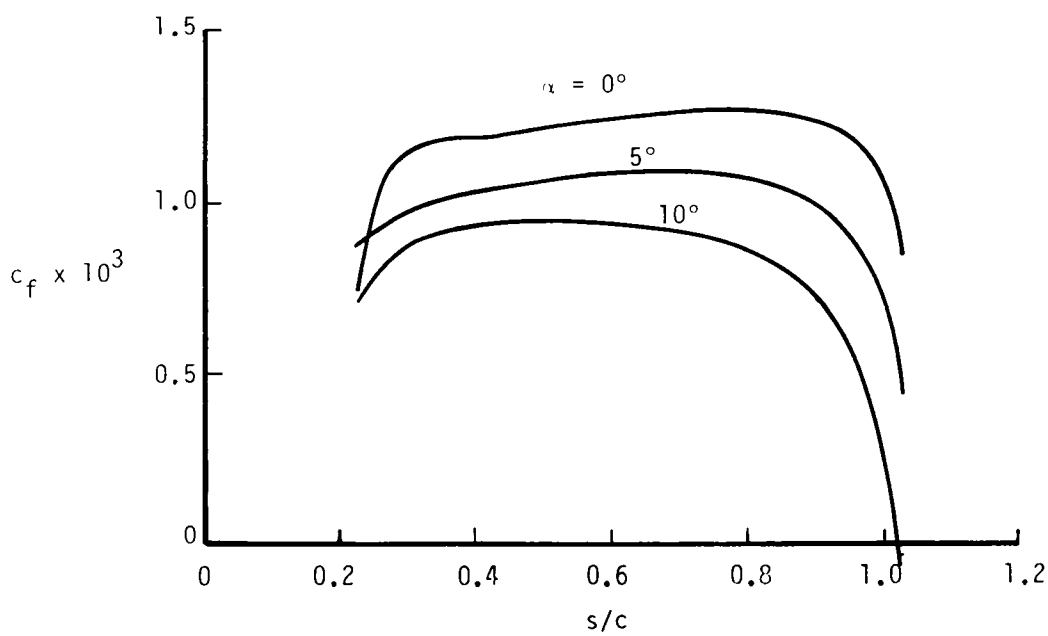

(b)

Figure 1. Variation of (a) displacement thickness δ* and (b) local skin-friction coefficient c_f for case 1, Eq. (19a), for k = 0.01.

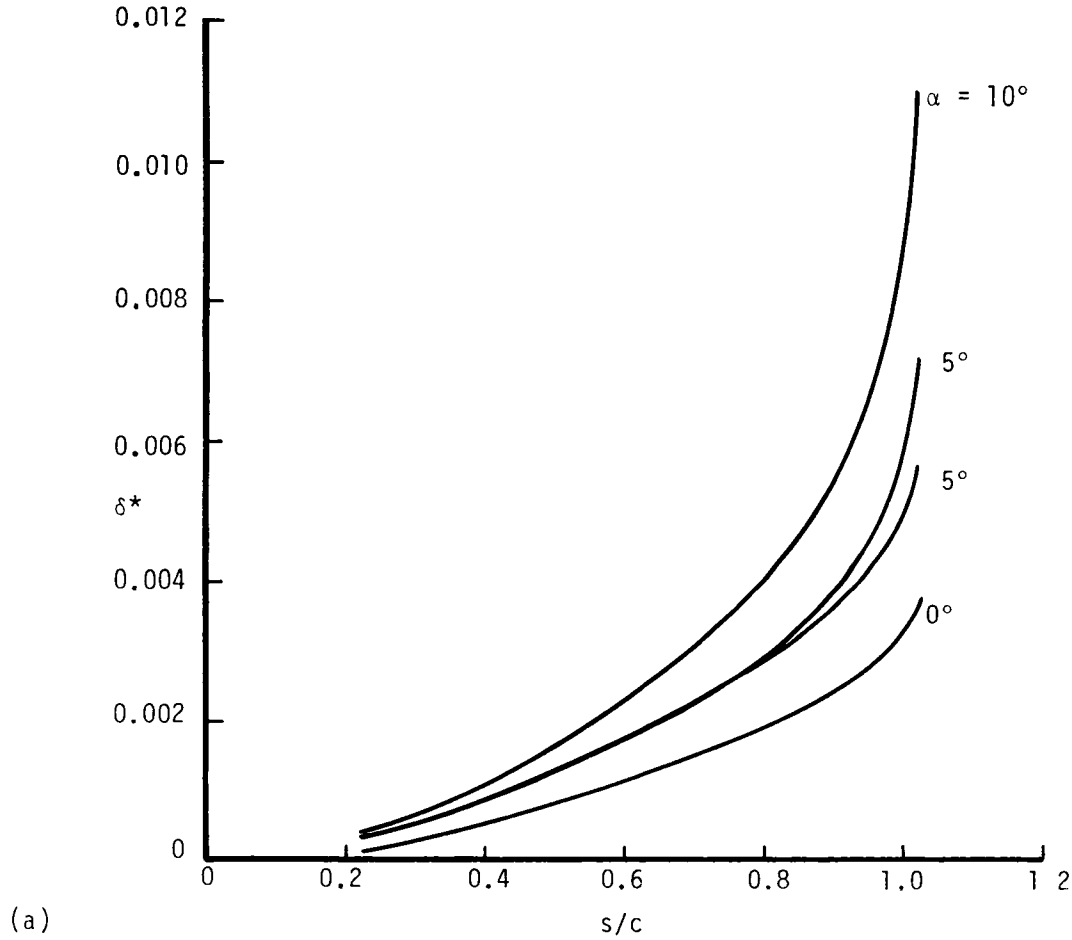

(a)

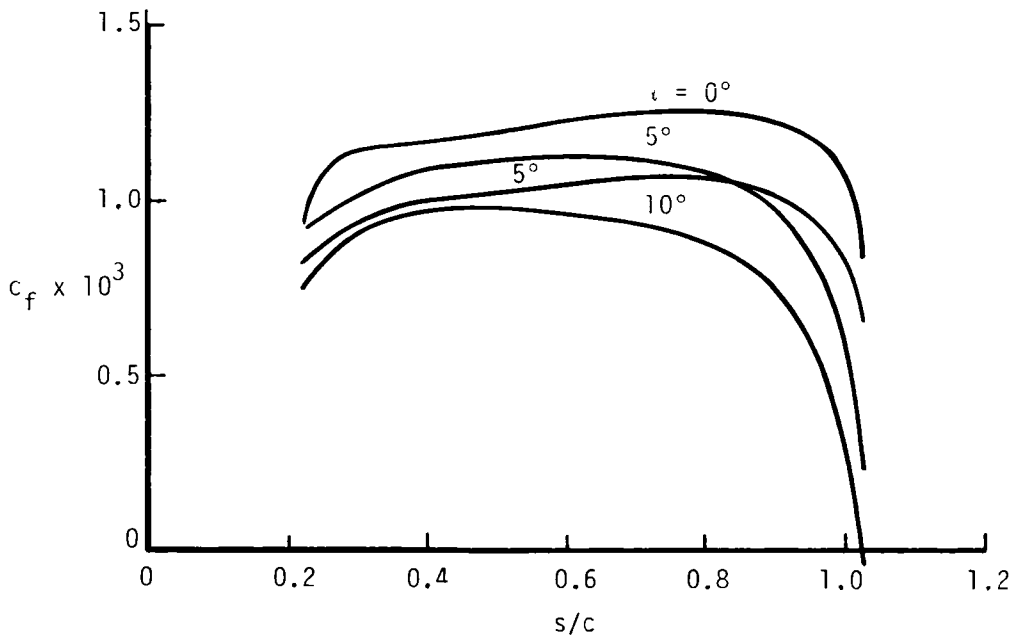

(b)

Figure 2. Variation of (a) displacement thickness δ* and (b) local skin-friction coefficient c_f for case 1, Eq. (19a), for k = 0.20.

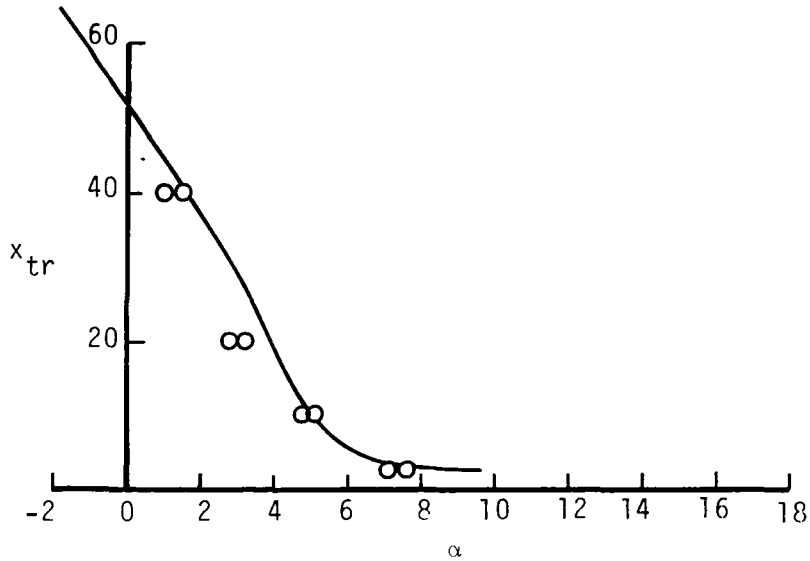

(a)

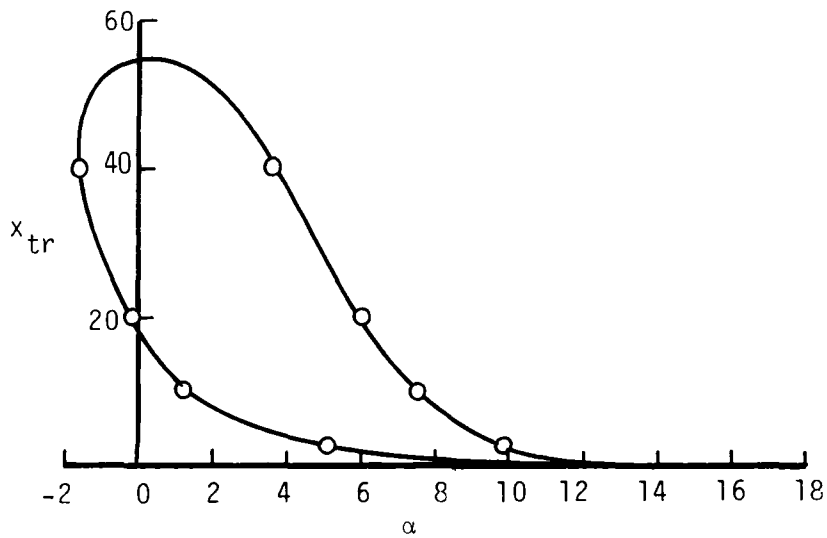

(b)

Figure 3. Variation of transition location with angle of attack on the NACA 0012 airfoil at two reduced frequencies: (a) k = 0.01, (b) k = 0.20, for case 2. The symbols denote experimental data of ref. 6 and the solid lines the fairing done by the authors.

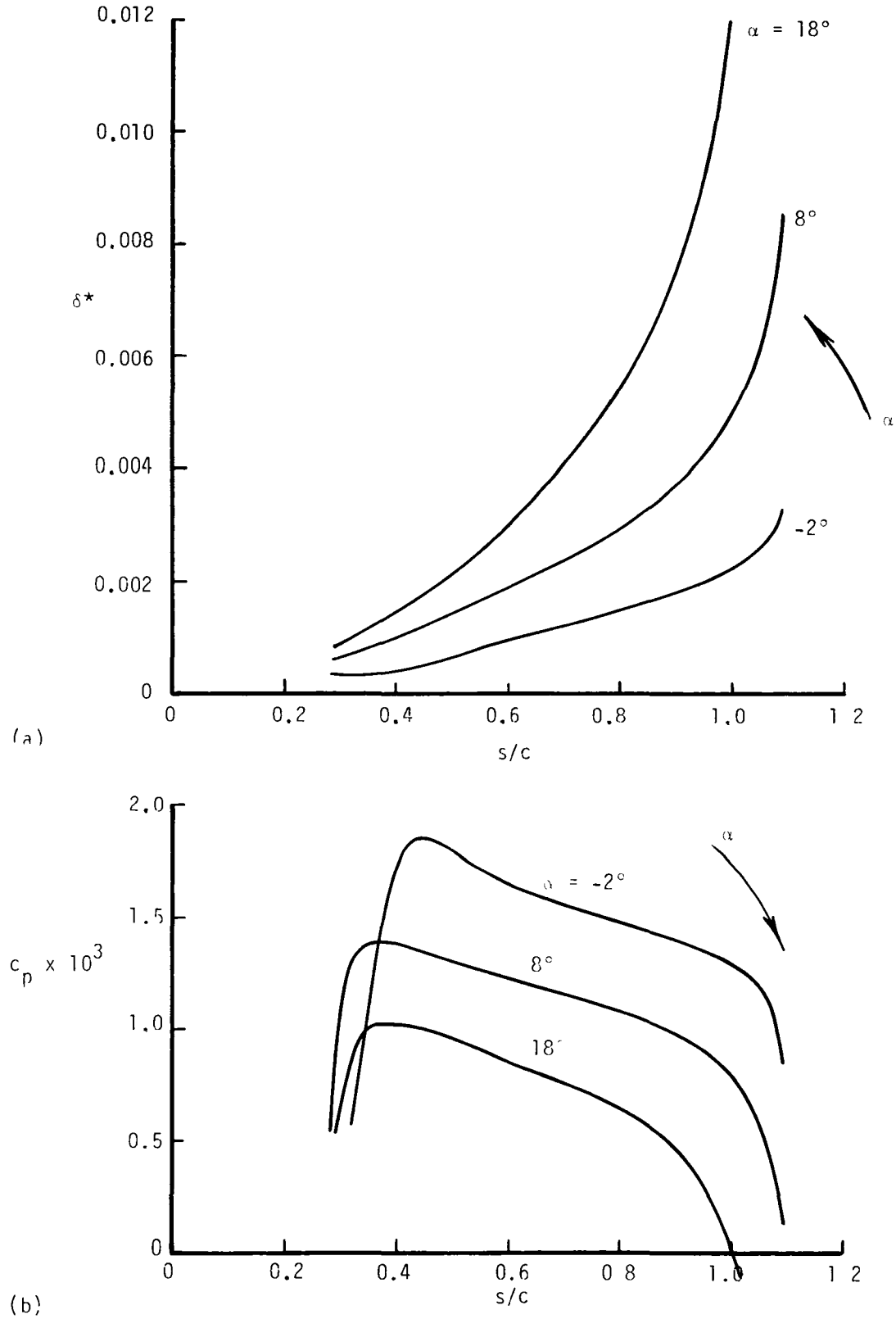

Figure 4. Variation of (a) displacement thickness, δ* and (b) local skin-friction coefficient c_f for case 2, Eq. (19b), for k = 0.01 with transition corresponding to maximum pressure peak. The arrow shows the upward stroke.

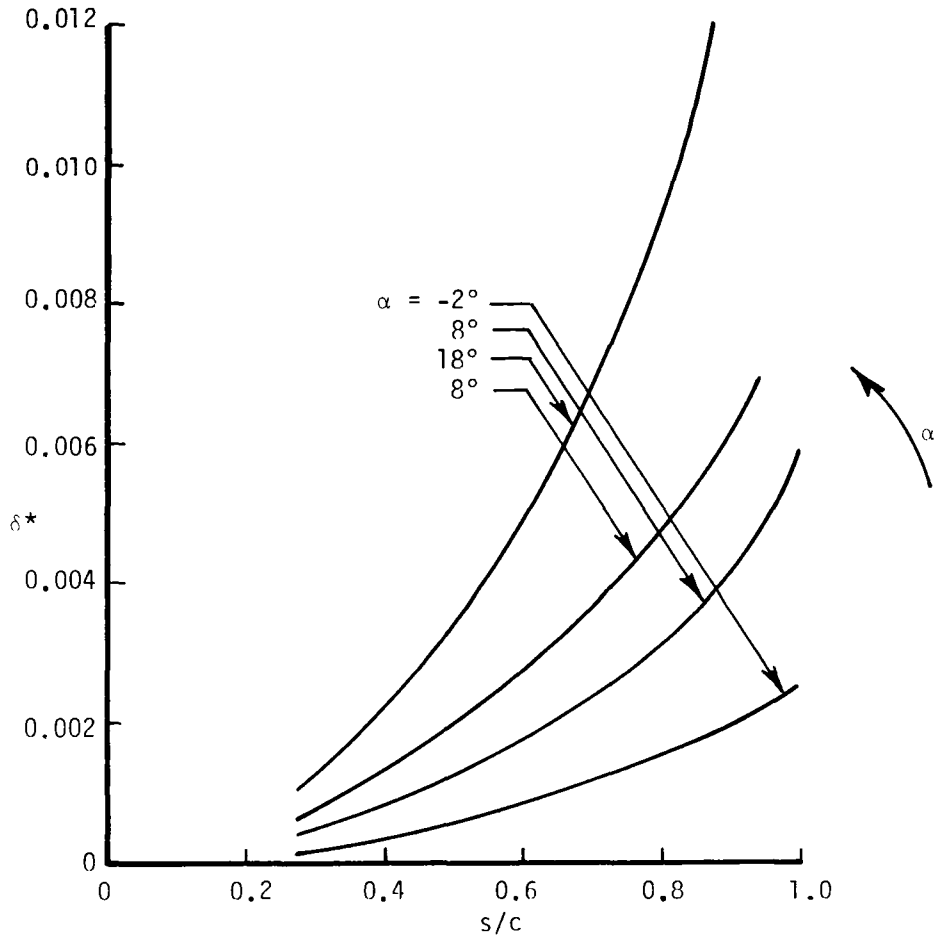

(a)

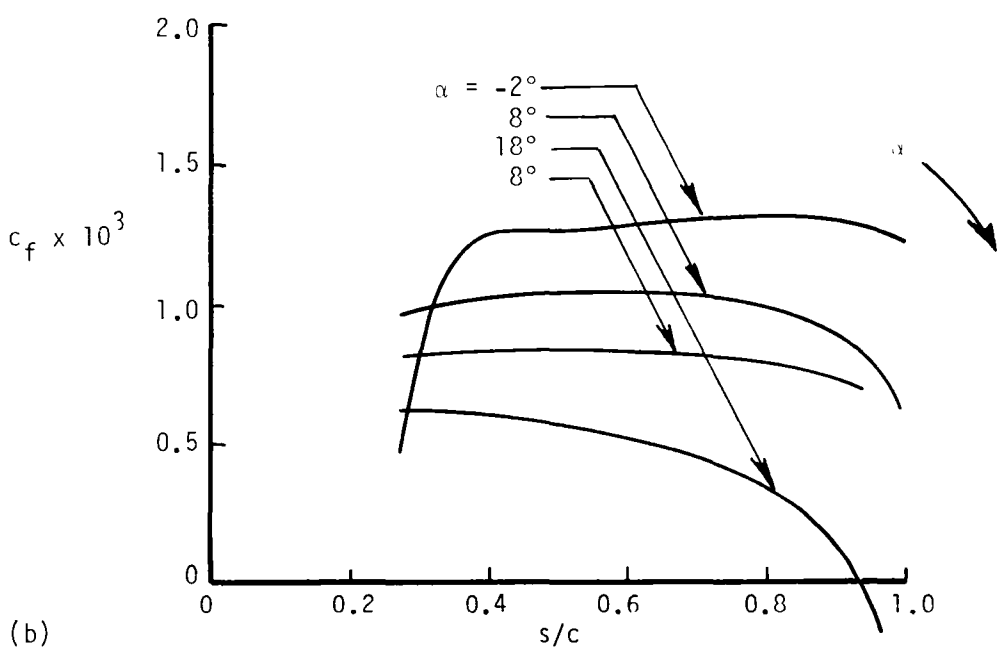

(b)

Figure 5. Variation of (a) displacement thickness δ^* and (b) local skin-friction coefficient c_f for case 2, Eq. (19b), for $k = 0.20$ with transition corresponding to maximum pressure peak. The arrow shows the upward stroke.

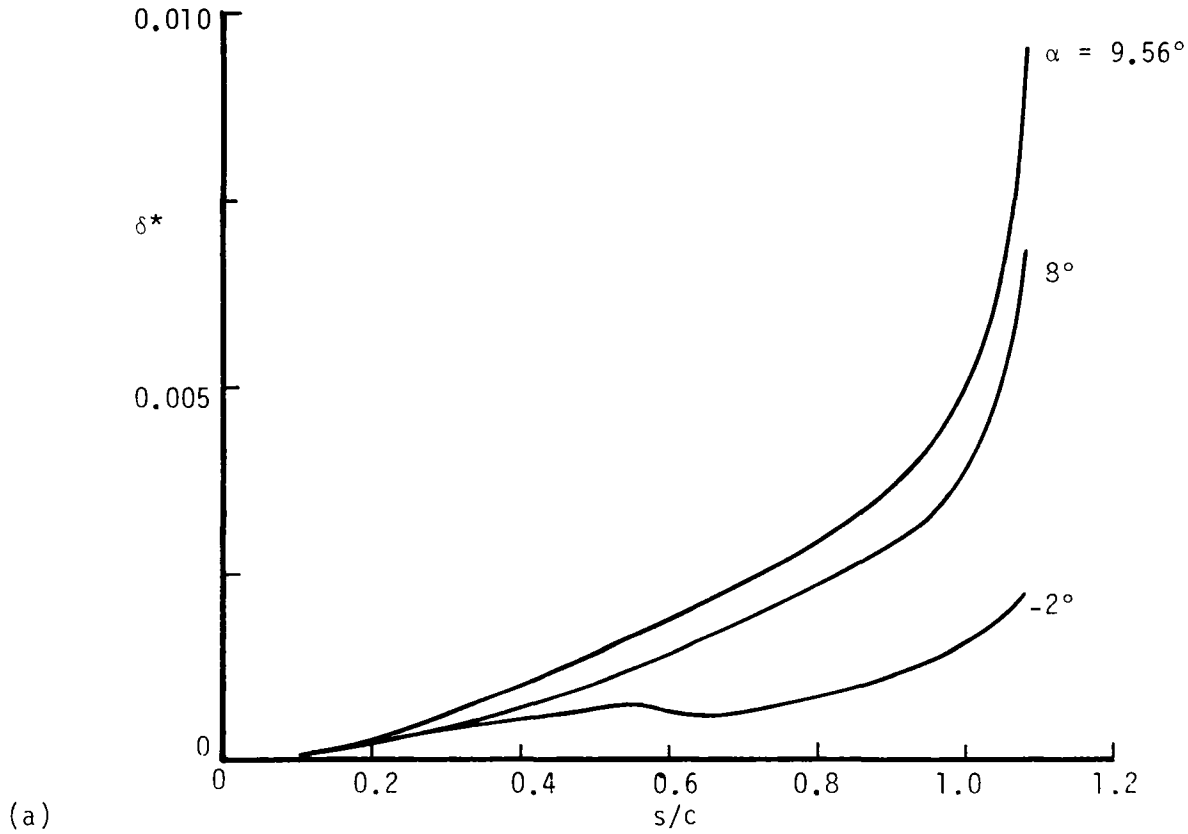

(a)

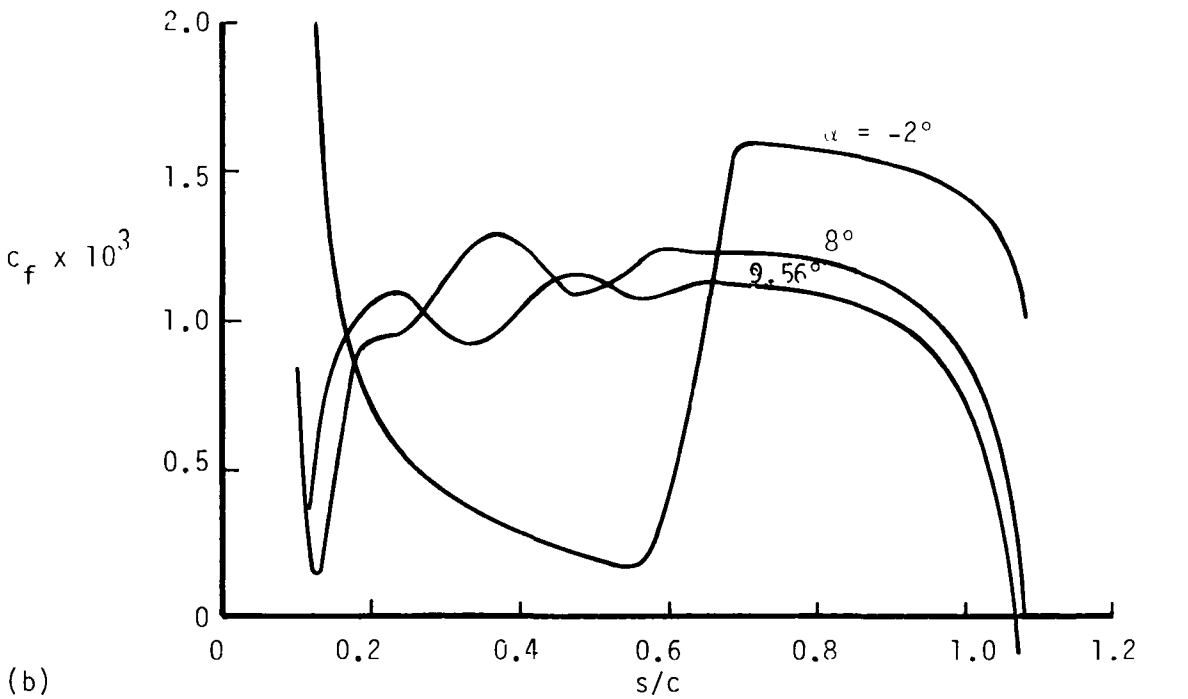

(b)

Figure 6. Variation of (a) displacement thickness δ* and (b) local skin-friction coefficient c_f for case 2, Eq. (19b), for k = 0.20 with transition specified according to the experimental data, Fig. 3b.

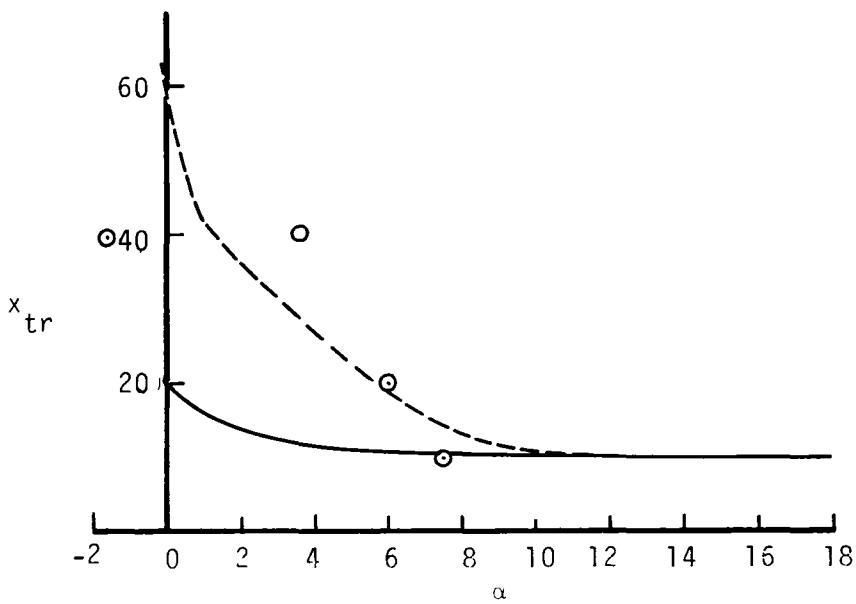

Figure 7. Comparison of experimental (symbols) and calculated (dashed line) transition locations together with those corresponding to maximum pressure peak (solid line) for upward stroke of case 2.

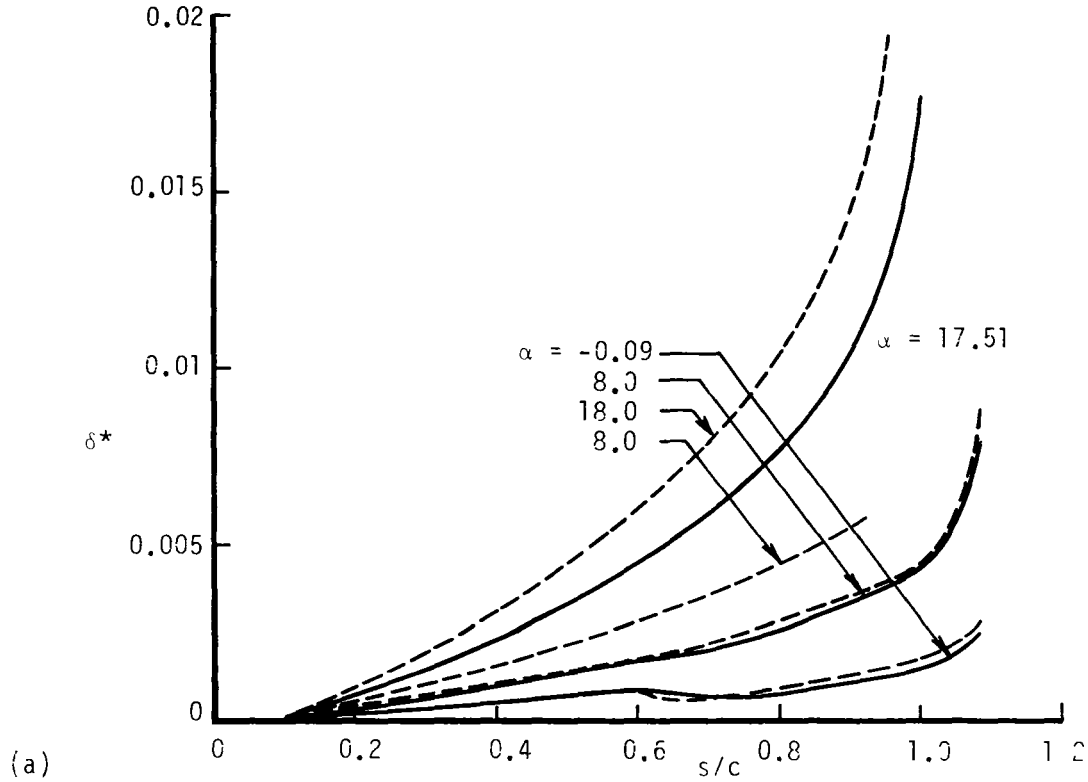

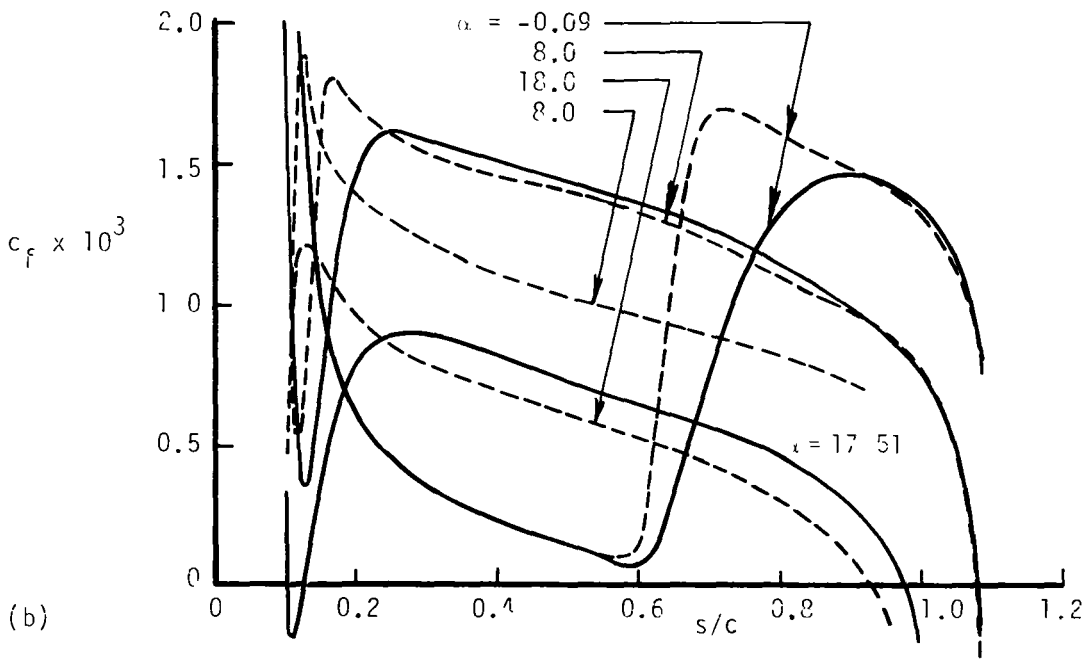

Figure 8. The effect of the intermittency expression on (a) displacement thickness δ*, and (b) local skin-friction coefficient c_f for case 2. Transition was calculated by Michel's method. Solid lines denote those computed with the coefficient of G equal to 1/1200 and dashed lines with 1/120.

1 Report No	2 Government Accession No	3 Recipient's Catalog No
NASA TM-85943		

4 Title and Subtitle	5 Report Date
CALCULATION OF BOUNDARY LAYERS OF OSCILLATING AIRFOILS	May 1984
	6 Performing Organization Code ATP
7 Author(s) Tuncer Cebeci* and Lawrence W. Carr**	8 Performing Organization Report No A-9599
9 Performing Organization Name and Address *Mechanical Engineering Dept., California State University, Long Beach, CA 90840 and **Ames Research Center and Aeromechanics Laboratory, U S Army Research and Technology Laboratories – AVSCOM, Ames Research Center, Moffett Field, CA 94035	10 Work Unit No T-4033Y
	11 Contract or Grant No
12 Sponsoring Agency Name and Address National Aeronautics and Space Administration, Washington DC 20546 and U.S. Army Aviation Systems Command, St Louis, MO 63120	13 Type of Report and Period Covered Technical Memorandum
	14 Sponsoring Agency Code 505-31-32

15 Supplementary Notes

Point of Contact: Lawrence W. Carr, Ames Research Center, MS 227-8, Moffett Field, CA 94035 (415) 965-6265 or FTS 448-6265

16 Abstract

A two-point finite difference unsteady laminar and turbulent boundary layer computational method has been used to investigate the properties of the flow around an airfoil (NACA 0012) oscillating through angles of attack up to 18 degrees, for reduced frequencies of 0.01 and 0.20. The unsteady potential flow was determined using the unsteady potential flow method of Geissler. The influence of transition location on stall behavior was investigated, using both experimentally determined transition information, and transition located at the pressure peak, the results show the need for viscous-inviscid interaction in future computation of such flows

17 Key Words (Suggested by Author(s))	18 Distribution Statement
Unsteady flow	Unlimited Subject Category - 34

19 Security Classif (of this report)	20 Security Classif (of this page)	21 No of Pages	22 Price*
Unclassified	Unclassified	28	A03

*For sale by the National Technical Information Service, Springfield, Virginia 22161

End of Document